Experimental study of the unsteady aerodynamics during flapping flight of birds: European Starling, Western Sandpiper and American Robin

Segreto, John M.[1,*]; Kirchhefer, Adam J.[2]; Hackett, Erin E.[1]; Guglielmo, Chris G.[2]; Kopp, Gregory A.[3]; Gurka, Roi[1,2];

[1]School of Coastal and Marine Systems Science, Coastal Carolina University, Conway, SC, USA
[2]Advanced Facility for Avian Research, University of Western Ontario, London, ON, Canada
[3]Boundary Layer Wind Tunnel Laboratory, University of Western Ontario, London, ON, Canada
[*]corresponding author: jmsegret@g.coastal.edu

Abstract
Birds' unique characteristics such as wing shape, flexibility, feathers, flapping motion, etc., result in high aerodynamic performance. Using various flight modes such as gliding, bounding, and flapping, birds can use a single propulsion system for multiple functions. In low Reynolds number flyers using flapping flight mechanisms, the contribution of unsteady effects on lift and drag is not entirely understood. To gain insight about the unsteady contributions, a controlled study on the near wake flow behind freely flying birds was performed. Long duration, time resolved particle image velocimetry (PIV), combined with high speed imaging has been used to characterize the various flow features in the wake that are associated with flapping flight. The specially designed PIV system can sample the flow field for twenty minutes yielding a continuous measurement, sampling several wingbeat cycles consecutively. Time series of the vorticity fields have been expressed as composite wake plots, which reveal various characteristics of the wake during the upstroke (US) and downstroke (DS) phase of the flapping as well as the transition between US to DS and vice versa. Comparison between the near wake fields behind the three birds show remarkable similarity in their wake structure. We have identified over multiple wing beat cycles the presence of what appears to be an overlap of two distinct wakes during the transition from US to DS, named "double branch". Over the region of the double branch, the majority of net positive circulation is accumulated. Indicating this may be a key feature in producing lift, and thus contribute to the observed high aerodynamic performance.
Keywords: birds' aerodynamics, high-speed PIV, wind tunnel, wakes

1 Introduction

The recent advances in the development of small UAVs (or MAVs) have prompted much research in the aerodynamics of flapping wings [1]. In the low Reynolds number region where these vehicles operate stationary wing configurations typically suffer, while birds as well as bats and insects with flapping wings have high performance capabilities[2][3]. Birds have the ability to vary wing geometry, which allows for multi-mode flight and the capability of generating vortex structures that enable high propulsive and lifting properties[3].

To measure the aerodynamic forces on odd shapes with unsteady motions one has to analyze the properties of the vortex structures or wake formed by the body[4]. In the past few decades wake configurations behind flapping birds' wings (so-called "gaits") have been described using idealized models, in order to better characterize the flow dynamics. These wakes have been described by theoretical models and reinforced by visualization techniques. The vortex ring gait was described in hovering flight[5] and slow forward flight[6][7] while at higher flight speeds the continuous vortex gait dominates[6][8][9][10]. The vortex ring gait proposes that each wing beat is aerodynamically active on the down stroke only. During the downstroke, tip vortices connect the starting and stopping vortices, creating an elliptical vortex ring, with no shedding of vorticity into the wake during the upstroke. Whilst, the continuous vortex gait model states that vorticity is shed continuously throughout the upstroke and downstroke without strong concentrations of starting or stopping vortices. The wake is dominated by tip vortices of nearly constant circulation. It is shown that the description of these gaits as discrete is somewhat incomplete; there is not an abrupt change between the two gaits instead the change is gradual over the speed range[4][11][12].

Advances in technology have allowed for quantitative measurements of the wake using Particle Image velocimetry (PIV). This method has been applied to a number of flying species, where measurements were taken at distances between 8 and 22 chord lengths[13]. These measurements have been applied to calculate the momentum balance using a quasi-steady aerodynamic assumption[14]. Using this approach, prior interactions of the near wake are neglected allowing for the assumption that the flow did not dissipate significantly in the streamwise direction; the wake is self-preserving at the far wake region[15]. Neglecting the unsteady affects however is not entirely justifiable for most flight conditions encountered in the low Reynolds number region for which unsteady aerodynamic effects are still significant[16][17]. At low Reynolds numbers, the flow may develop wake-wake interactions that can potentially cause cancellation of vorticity and reconnection of vortex lines that can significantly modify the qualitative and quantitative properties of fluid flows[4].

To better understand the interactions of fluid structures in the near wake of avian flight, models instead of living animals have been used. A model was developed by Ruck et al.[18] (2010) to investigate the unsteady and turbulent effects on aerodynamic performance for flapping wings. At reduced frequencies of 0.22, which is similar to that of many birds flying at cruising speed, it was found that tip and root vortices dominate the wake pattern. Throughout the entire downstroke it was found that there is a well pronounced root vortex while the vortex sheet separates more quickly at the tip. It is not until the upper reversal point that the root vortex begins to separate. The small scale vortex structures that are shed continuously and the bound vortex that is present throughout the downstroke and upstroke decrease the strength of the starting and stopping vortices as well as spanwise structures. Behind the body secondary vortex structures were observed with minimal strength when compared to the vortices generated by the wings and thus it was concluded that their effects can be neglected[18]. This flow can be compared with the continuous vortex gait where vorticity is shown to follow only the path of the wing tips at large spanwise distances from the origin of the wake.

In the present experiment, a controlled study on the near wake flow behind freely flying birds was performed. Three birds were chosen for the experiment increasing the number of species for which PIV data is available at the same time allowing for comparison between near wakes of several species. High spatial and temporal resolution was accomplished by having a relatively small field of view and sampling at 1000 Hz yielding 500 vector maps per second. High temporal resolution allows for many measurements of the same wing beat cycle while high spatial resolution allows for more accurate description of the qualitative and quantitative characteristics of the wake. Measurement in the near wake may support the numerical model of

fluid structure interactions, while comparing the near and far wakes behind freely flying birds will allow for a deeper understanding of the wake development in the streamwise flow.
To study the interaction between turbulence and birds' flight the European Starling, Western Sandpiper and American Robin were chosen. Time series of the vorticity fields have been expressed as composite wake plots, which depict segments of the wing beat cycle for various span-wise locations in the wake. Comparison between the near wake fields behind the three birds reveals remarkable similarity in their wake structure. We have identified over multiple wing beat cycles the presence of what appears to be the interaction between root and tip vortices described as a double branch feature. A quantitative analysis of the vorticity field has shown that the double branch feature yield a net increase in positive circulation. In the near wake, unsteady features can be observed while allowing for a better understanding of how the wake develops. This understanding will allow for better calculations and force balances that cannot be accomplished at large streamwise distances where the flow is fully developed and unsteady effects and dissipation cause losses.

2 Experiments

Animals: Three distinct birds were tested in the AFAR facility. The bird species were: European Starling (Sturnus vulgaris), Western Sandpiper (Calidris mauri), and American Robin (Turdus migratorius). Morphological parameters of the birds, as well as parameters of the experiment, are summarized in Table 1. All birds went through similar training sessions before data were recorded. Specially designed safety goggles (Yamamoto Cogaku Co. YL 600) were worn by the birds while flying in the tunnel. A set of optoisolators operated by six infrared transceivers were integrated into the PIV system in order to prevent direct contact between the bird and the laser sheet. The optoisolators triggered the laser only when the bird was flying upstream from the PIV field of view. Animals' care and procedures were approved by the University of Western Ontario Animal Use Sub-Committee (protocols 2006-011, 2010-2016).

Table 1: Bird's physical specifications

Bird	Weight [gr]	Wingspan [cm]	Chord [cm]	Wind speed [m/sec]	Wingbeat frequency [Hz]	Reynolds number	Strouhal number	Reduced frequency
Starling	78	38.2	6	13.5	12.6	5.4×10^4	0.18	0.17
Robin	78	42.8	10.6	12	11.9	8.6×10^4	0.37	0.33
Sandpiper	30.3	25.5	4.5	10	12.8	3.1×10^4	0.19	0.18

Wind tunnel: The experiments were performed at the hypobaric climatic wind tunnel at the Advanced Facility for Avian Research (AFAR) at UWO. The wind tunnel is a closed loop type with an octagonal test section of 1.2m preceded by a 2.5:1 contraction. The turbulence intensity at the test section was smaller than 0.3% with a uniformity of 0.5%. The wind tunnel allows the control of speed, pressure, temperature and humidity. The bird is introduced into the test section through an opening that is located between the downstream end of the test section and the diffuser. The flight conditions for all birds were at atmospheric pressure, a temperature of 15°C, and relative humidity of 80%.

PIV: Long-duration time-resolved PIV system [19] was employed for the wake flow measurements. The PIV system consists of a 80 W double-head diode-pumped Q-switched Nd:YLF laser at a wavelength of 527 nm and two CMOS cameras (Photron FASTCAM-1024PCI) with spatial resolution of 1024x1024 pixel^2 operating at a rate of 1000 Hz. The PIV system is capable of acquiring image pairs at 500 Hz using two cameras for 20 minutes continuously. Olive oil particles, 1μm in size were introduced into the wind tunnel using a Laskin nozzle from the downstream end of the test section so no disturbance was caused to the flow or to the bird.
Herein, we used one camera for the PIV whilst the other camera was used simultaneously for measuring the wingbeat kinematics. The PIV camera's field of view (FOV) was 12x12 cm^2 for the starling and sandpiper experiments corresponding to 2c by 2c, where c is the Starling chord length and 2.6c by 2.6c for the sandpiper. The PIV FOV for the robin data was 14x10 cm^2 (1.4c x 1c). The velocity fields were computed using OpenPIV (Taylor et al., 2010) using 32x32 pixel^2 interrogation windows with 50% overlap, yielding a spatial resolution of 32 vectors per average chord, equal to 1.8 vectors/mm. In the sandpiper experiments, a total of 2600 vector maps were recorded, and out of this dataset 500 vector maps contained features of the

near wake behind the bird's wing, 1000 and 700 vector maps were recorded for the starling and the robin respectively where 400 and 300 were used for the analysis of the wake features of both birds. The measured wake was located 4 wing chord lengths behind the right wing. The wake was sampled in the parasagittal plane at 2 ms intervals (500 Hz), therefore, both the downstroke and the upstroke phases were temporally resolved.

Kinematics: Wingbeat kinematics were recorded using high-speed CMOS camera operating at 1000Hz with a spatial resolution of 1000x1000 pixel^2. The field of view was equal to 46x46 cm^2, corresponding to an area of 9c by 9c for both the sandpiper and the starling whilst for the robin it was 74x74cm^2 (7c × 7c). From the images we calculate the wingbeat frequency where the wingtip is identified its amplitude is calculated from the high speed images by estimating the wingtip motion between the consecutive images. The kinematic images were synchronized with the PIV images in order to provide a direct relation between the wake formed by the motion of the wing and its kinematics. In addition, a floor-mounted camera operating at 60 Hz was used to record the spanwise position of the bird in respect to the laser sheet illumination. These images provided the identification of the measured PIV plane and its location in respect to the wing; so that, the wake velocity fields were associated with the spanwise location across the wing. The floor-mounted camera was not synchronized with the PIV or the kinematic measurements; therefore the two time histories were synchronized manually based on the presence of the laser light in the images. Once synchronized, spanwise positions were assigned to the wake data acquired at 500 Hz based on interpolation from the simultaneously recorded spanwise positions.

Error estimation: An error analysis based on the root sum of squares method has been applied to the velocity data and the wing kinematics. The errors were estimated as: 2.5% for the instantaneous velocity values, 10% for the instantaneous vorticity and 4% for the circulation, which was calculated, based on the vorticity field. The error introduced in the kinematic analysis resulted from the spatial resolution of the image and the lens distortion leading to an estimated error of 5% in the wing displacements.

3 Results

Kinematics

Each of the three species has a wing beat frequency between 11.36 and 13.16 Hz. The duration of wingbeat cycle that consisted of four stages: upstroke, transition from US to DS, downstroke and finally transition from DS to US. Dividing the entire wingbeat cycle into two main regions: upstroke and downstroke, shows that for the three birds, the period for both phases is approximately equal. Yet, if one chooses to classify the entire cycle from a transitional point of view; where The USDS is defined as the period for which the mid-wing is above the horizontal body plane, while the DSUS is the period where the mid-wing is below the plane. Than the USDS was approximately 60% of the cycle while the DSUS was 40%. The kinematic data of each wingbeat cycle is described in table 2 where the upper amplitude and lower amplitude are defined as the height the wingtip is above or below the center of the body at the reversal points.

Table 2: Kinematic parameterization of the flapping mode

Bird	Frequency (Hz)	DS (%)	US (%)	USDS (%)	DSUS (%)	Upper Amp. (c)	Lower Amp. (c)	Speed (m/s)
Robin	13.16	53	47	58	42	2.1	1.5	11
Western Sandpiper	11.36	43	57	61	39	1.8	1.7	10
Starling	12.82	54	46	54	46	.5	2.7	13.5

The discussion of an entire wing beat cycle requires that the flow be divided into phases as well as noting the spanwise location of the wake. In figure 1 the images are in sequential order from right to left as the bird goes through one full wingbeat cycle. From position '*e*' to '*d*' will be considered the lower upstroke region, '*d*' to '*c*' the upper upstroke region, '*d*' to '*b*' will be considered the upstroke to downstoke transition (USDS), '*c*' to '*b*' and '*b*' to '*a*' are then the upper and lower downstroke region respectively, from '*b*' to '*d*' is then the downstroke to upstroke transition (DSUS). The entire upstroke (US) is considered as '*e*' to '*c*' and the downstroke (DS) is from '*c*' to '*a*'.

Fig. 1: Instantaneous images describing the full wingbeat cycle of a Sandpiper

In order to describe the wake and how it was formed it is important to note the location and position of the birds' wings with respect to the PIV imaging plane. This allows for the correlation between the point where the disturbance in the flow was created and the point at which the wake was measured. To associate the kinematic data with the PIV realizations the calculated convection velocity and the distance between the wing and the measurement plane were used.

Flow measurements

To visualize the flow in the PIV realizations the mean free stream velocity is subtracted from the instantaneous measurements so that the disturbance created by the bird is more apparent and it appears as if the bird flew through still air. The vector maps are then superimposed over the vorticity, ω, contour maps (as shown in figure 2).

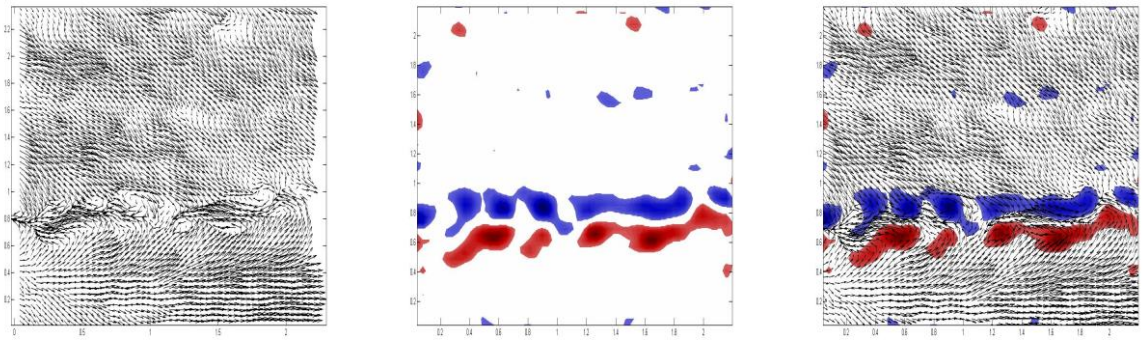

Fig. 2: Instantaneous velocity and vorticity fields of the wake formed by the bird motion during flapping: a) instantaneous velocity b} instantaneous vorticity and c) superimposed vorticity over the velocity maps.

The spanwise vorticity, which will be used as the characteristic quantity in the wake visualization, is calculated as:

$$\omega = \frac{\partial v}{\partial x} - \frac{\partial u}{\partial y} \qquad (1)$$

In order to complement the wake vortices and the wake reconstruction (as described later), we have estimated the circulation. This estimate enables the association of some of the flow patterns with the different phases of the wingbeat cycle as one may expect to obtain net positive circulation as the bird gains lift (mostly during the downstroke phase), and net negative circulation over most of the upstroke.
To calculate the circulation, the center of each vortex was identified, and then the boundary of the vortex was

determined. Vortex cores were identified by using a threshold of 1% of the maximum vorticity over the wing beat cycle. Once the location of the maximum vorticity was identified, a neighborhood search was applied to determine the boundaries of the vortex. The boundary of the vortex was then determined as any point with less than 25 percent of the vorticity of the core or any point that was greater than 115% of a consecutive point closer to the core. Once each vortex was identified the circulation, Γ, of the vortex was calculated as:

$$\Gamma = \sum \omega_{ij} A \qquad (2)$$

The circulation was calculated based on averaging four consecutive regions in every instantaneous voriticy map. This was accomplished by breaking each vorticity map into four vertical sections based on the instantaneous convection velocity. The circulation was then calculated for each section defining the location of the vortex as within that section if the vortex core was within the section. This allows for the total circulation over the wing beat cycle to be calculated for each time the flow features were captured. Averaging these values together gives a more accurate picture of the circulation of the flow features. In figure 3a the dotted lines are the circulation calculated (positive and negative calculated separately) for each time the flow features were captured, while the solid lines are the averaged value. In Figure 3b the sum of the positive and negative circulations is shown, and in figure 3c the cumulative sum of the circulation up to that point, meaning each point is the sum of the circulation calculated at that point plus the circulation of every point that came before it (to the right).

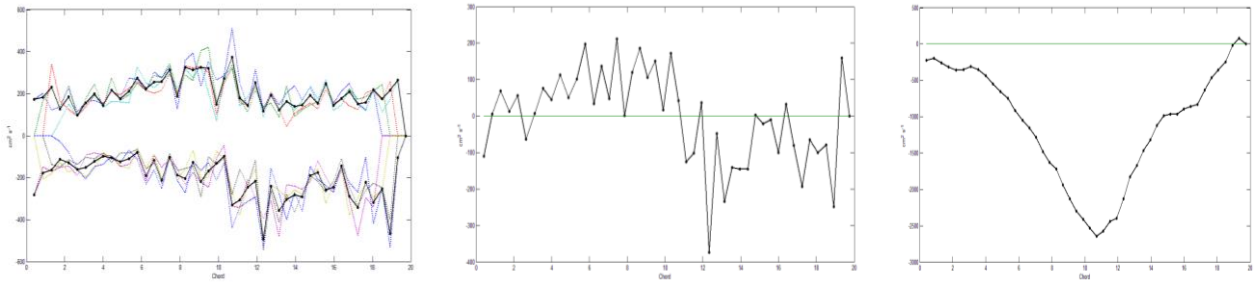

Fig. 3: Cumulative circulation at the sandpiper wake region; a) circulation where positive and negative calculated separately and the solid lines are the averaged value, b) the sum of the positive and negative circulations, c) the Cumulative circulation for the wake evolution

Convection Velocity

The convection velocity is calculated by comparing consecutive PIV realizations using a spatially averaged time correlation[13]. The data is sampled at 500 Hz allowing for flow features to be captured several times and allowing for consecutive images to "overlap") by approximately 75 percent. This overlap lends itself to use this correlation technique to quantitatively compare wake features to determine the degree to which they have convected through the flow.

The correlation quantitatively describes the degree to which the two velocity fields are the same. The shift that results in the maximum correlation coefficient is thus the distance that the wake has convected through the flow. The convection velocity is then calculated by examining the distance the flow features traveled in the time between the two consecutive images.

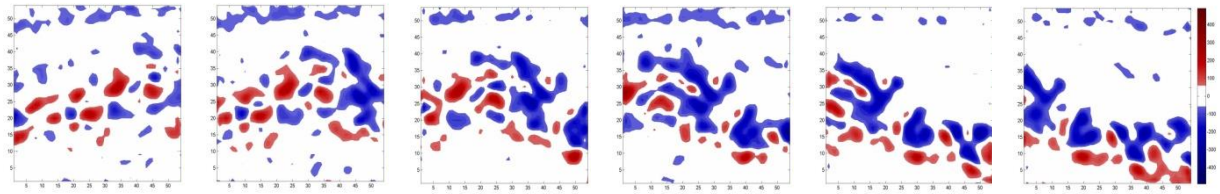

Fig. 4: Consecutive vorticity maps extracted from the high-speed PIV demonstrating the wake evolution

In figure 4 consecutive vorticity maps that were extracted from the high-speed PIV image show the flow being convected from left to right through the field of view. One can observe that the same flow feature is captured in at least five images. Therefore, we can perform a correlation analysis to find the optimal matching between these images. The spatially averaged time correlation coefficient is defined as:

$$C(X,Y,T) \approx \sum_{i=1,j=1}^{I,J} \frac{[w'(x_i,y_j,t)-\mu(t+T)][w'(x_i+X,y_j+Y,t+T)-\mu(t+T)]}{IJ\sigma(t)\sigma(t+T)} \quad (3)$$

Where C is the correlation coefficient between a velocity field at time t and the velocity field at a later time ($t+T$), spatially offset to a different location by the distance X and Y. The quantity $w'(x_i, y_j, t)$ is a component of the velocity vector at the spatial location (x_i, y_j). The indices i and j represent elements of the I by J grid of velocity vectors in which $w'(x_i, y_j, t)$ and $w'(x_i+X, y_j+Y, t+T)$ overlap. The variables $\sigma(t)$ and $\sigma(t+T)$ are the standard deviations of the velocity field at time t and time $t+T$ respectively. Because the two velocity fields are recorded in the PIV field of view, a finite measurement area, any spatial shift during the evaluation of C (due to variables X and Y) will result in a different area in which all contributing terms of C can be evaluated. For this reason, the average and standard deviation of each velocity field are evaluated, in the region where $w'(x_i, y_j, t)$ and $w'(x_i+X, y_j+Y, t+T)$ overlap, for every spatial shift (X and Y) for a given value of T.

Wake Composite

Reconstruction of the wake allows one to depict the wake topography over a long distance, thus shedding light on the various flow structures that form due to the wing flapping motion. The utilization of the long duration time resolved PIV system enables the reconstruction of the wake evolving behind the wings for a relatively long time with high spatial and temporal resolution.
The reconstruction is based on the PIV images taken from a stationary camera yielding Eulerian observation of the flow field. The birds fly from left to right; therefore the downstream distance is measured as positive chord lengths. What appears as downstream essentially happened earlier while what appears as upstream happened later. Throughout each wing beat cycle the birds position did not change much relative to the measurement plane. Thus invoking Taylor's hypothesis allows for the assumption that the flow remains relatively unchanged as it passes through the measurement plane. To visualize an entire wing beat cycle a wake composite image is generated by offsetting each consecutive PIV image by the calculated instantaneous convection velocity and overlapping the images keeping the closest section of the image to the bird, essentially the youngest part of the wake. Determining the beginning and end of the wing beat cycle was accomplished by analyzing the kinematics and associating them with their corresponding section of the wake. It was found that each wing beat cycle was spanning between 12 and 20 cord lengths for the various wakes analyzed. Three distinct wakes were analyzed for the three birds. Each of the wakes share many similarities and differences. These differences can be associated with the small differences in the kinematics of the wing beat cycle while the similarities provide some insight into a generalized wake model. Figure 5 present the three wake reconstructions demonstrating the evolution of the wake flow behind the freely flying birds. The contours represent the vorticity field imposed on the velocity field depicted as 2D vectors. The axes are scaled based on the specific bird's chord length. Beneath each wake composition, the cumulative circulation is given to show the relationship between the wake features and the resulting instantaneous circulation. Figure 5a depicts the wake from the Starling, figure5b represents the Sandpiper wake and the last (figure 5c) shows the robin wake. Each bird demonstrates some unique features in the wake topography yet the general description of the strong events as depicted in all the figures are similar.
In classical wakes behind airfoils (or bluff bodies) one would expect to obtain a vortex street[20], characterized by two alternating vortices opposite in sign, evolving in the streamwise direction further from the body. In our case, where the near wake of a flapping wing was measured, a vortex street is observed yet with some modifications, and complexity. In order to shed light on this peculiar pattern, a detailed description of these features for each of the examined wakes is described herein.

Western Sandpiper
The lower upstroke region consists of mixed vorticity that seems to be organized into two distinct branches with downwash throughout. These branches then become a single branch with strong coaxial flow, with backwash above and upwash below. This single branch region seems to contain high values of negative vorticity, populating the entire wake. At the USDS transition, the wake splits into a double branch region. Above and below this transition point is a strong upwash flow. The upper branch has strong coaxial flow throughout while the lower branch consists of some weak coaxial flow and some upwash flow. The lower branch begins to weaken while the upper branch begins to dominate and continue into a single branch region that persists through the lower downstroke region until some mixed vorticity begins. During the downstroke phase there is strong coaxial flow mixed with backwash and downwash.

Starling
At the beginning of the upstroke phase there is a single branch with weak coaxial flow, and strong backwash above and below the concentrated vorticity region. Then, an area of mixed vorticity with strong forward velocity is apparent. This section is followed by a section of strong seemingly coaxial flow although the vorticity is quite mixed without a clear shedding path. There is upwash flow above and below this region. The transition phase in the Starling wake is not as clear as in the case of the Sandpiper. The circulation figure assist in identifying this region, where the circulation changes its trend from negative towards positive. Throughout the transition from upstroke to downstroke there is a defined double branch region. The lower branch consists of some coaxial flow while the upper branch has mostly downward velocity, until the end of the double branch region where both the upper and lower branches both have strong coaxial flow. The branches then seem to merge into a single branch for a short period above and below this region there is much backwash, followed by an area of mixed vorticity with strong upwash throughout.

Robin
The beginning of the upstroke region has mixed vorticity. During the mid phase of the upstroke, a semi double branch is formed. Above the double branch there is backwash while below there is upwash flow. The pattern seems to be 'closing' and than reconfigure into a new double branch accompanied by strong coaxial flow, with downwash from above and upwash from below. There is some coaxial flow in the upper branch that seems to be pulled into the coaxial flow of the lower branch. The double branch then becomes a single branch with very strong coaxial flow throughout whilst backwash flow is apparent above and below it. In the downstroke phase there is mixed vorticity with strong downwash flow.

4 Discussion and conclusion

During the upstroke phase, as appears in the wake composites starting from the right side of the figures, the vortices shed are accompanied by mainly upwash flow with coaxial flow regions. Towards the end of the upstroke phase into the transition, a downwash flow start to appear followed by high values of negative vorticity compared to the positive ones. This section is followed by the formation of double branch[13] feature where four distinct vorticity contours, opposite in sign forming an apparent two vortical patterns aligned together. The transition from upstroke to downstroke phase (USDS) is governed by a double branch pattern. A strong upwash flow is observed in this region for the three wakes. Following the transition phase, the downstroke is characterized by downwash flow. In addition, the 'closing' of the double branch turns continuously into a single vortical pattern. Throughout the region of the double branch structure there is an accumulation of positive circulation indicated by the negative slope of the cumulative circulation plots.

The composition of the measured vorticity fields provides a quantitative description of the circulation at the near wake and is associated with the wing beat phases. Over multiple wing beat cycles the presence of a double branch feature is shown in the transition region from US to DS. It appears as if this feature is key in producing a net positive circulation over the wing beat cycle. Over the region of the double branch, in these continuously shed vorticity wakes, the majority of net positive circulation is accumulated. Indicating this may be a key feature in producing lift, and thus contribute to the high aerodynamic performance observed by these low Reynolds flyers.

6 References

[1] Han J H, Lee J S, Kim D K (2009) Bio-inspired flapping UAV design: a university perspective. *SPIE Smart Structures and Materials+Nondestructive Evaluation and Health Monitoring*, pp. 72951I.

[2] Lissaman P B S (1983) Low-Reynolds-number airfoils. *Annual Review of Fluid Mechanics,* vol. 15(1), pp 223-239.

[3] Rozhdestvensky K V, Ryzhov V A (2003) Aerohydrodynamics of flapping-wing propulsors. *Progress in Aerospace Science*, vol.39, pp 585–633.

[4] Spedding G R, Ros´en M, Hedenström A (2003) A family of vortex wakes generated by a thrush nightingale in free flight in a wind tunnel over its entire natural range of flight speeds. *Journal of*

Experimental Biology, vol. 206, pp 2313-2344.

[5] Rayner J M V (1979) A Vortex theory of animal flight. I. The Vortex wake of a hovering animal. *Journal of Fluid Mechanics*, vol. 91, pp 697-730.

[6] Rayner J M V, Gordon R (1998) Visualization and modeling of the wakes of flying birds. *Biona Report*, vol. 13, pp 165-173.

[7] Rayner, J M V (1979) A Vortex theory of animal flight. II. The forward flight of birds. *Journal of Fluid Mechanics*, vol. 91, pp 731-763.

[8] Spedding, G R (1987) The wake of a kesterel (Falcon tinnunculus) in flapping flight. *Journal of Experimental Biology*, vol. 127, pp 59-78.

[9] Spedding, G R (1986) The wake of a jackdaw (corvus monedula) in slow flight. *Journal of Experimental Biology*, vol. 125, pp 287-307.

[10] Hendenstom A, Rosen M, Spedding G R (2006) Vortex wakes generated by robins Erithacus rubecula during free flight in a wind tunnel. *Journal of Royal Society Interface*, vol. 3, pp 263-276.

[11] Rosén M, Spedding G R, Hedenström A (2004) The relationship between wingbeat kinematics and vortex wake of a thrush nightingale. *Journal of Experimental Biology*, vol. 207, pp 4255-4268.

[12] Hedenström A, Van Griethuijsen L, Rosen M, Spedding, G R (2006) Vortex wakes of birds: recent developments using digital particle image velocimetry in a wind tunnel. *Animal Biology*, vol. 56(4), pp 535-549.

[13] Kirchhefer A, Kopp G A, Gurka R (2013) The near wake of a freely flying European starling. *Physics of Fluids,* 25: 051902. doi: 10.1063/1.4807064

[14] Spedding G R, (1987), The wake of a kestrel (Falco tinnunculus) in flapping flight. *Journal of Experimental Biology*. vol. 125, pp 59–78.

[15] Haddadpour H, Firouz-Abadi R D (2006) Evaluation of quasi-steady aerodynamic modeling for flutter prediction of aircraft wings in incompressible flow, *Thin-Walled Structures*, vol. 44, pp 931–936.

[16] Mueller T J, DeLaurier J D (2003) Aerodynamics of Small Vehicles. *Annual Review of Fluid Mechanics*, vol. 35, pp 89-111.

[17] Hedenström A, Spedding G R (2008) Beyond robins: aerodynamic analyses of animal flight. *Journal of Royal Society Interface*, 20085, pp 595-601;DOI: 10.1098/rsif.2008.0027.

[18] Ruck S, Oertel H (2010) Fluid-structure interaction simulation of an avian flight model. *Journal of Experimental Biology*, vol. 213, pp 4180-4192.

[19] Taylor Z J, Gurka R, Kopp G A, Liberzon A (2010) Long-duration time-resolved PIV to study unsteady aerodynamics. *IEEE Transactions on Instrumentation and Measurement*, vol. 59(12), pp 3262-3269.

[20] Roshko, A (1954a) On the drag and shedding frequency of two-dimensional bluff bodies, *NACA Technical Note 3169*.

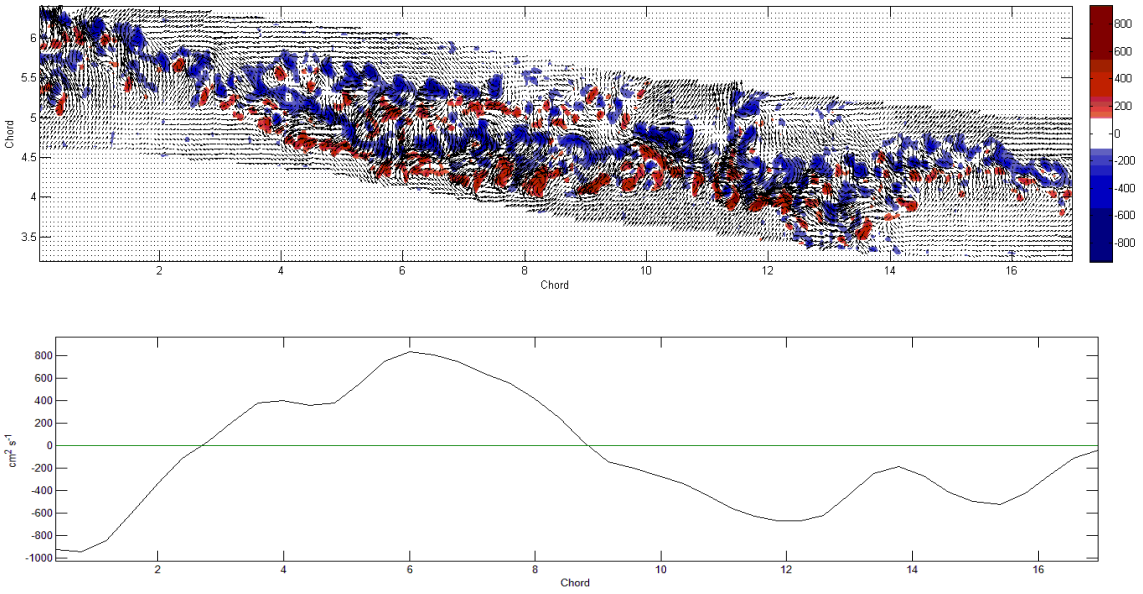

Fig 5a: European starling

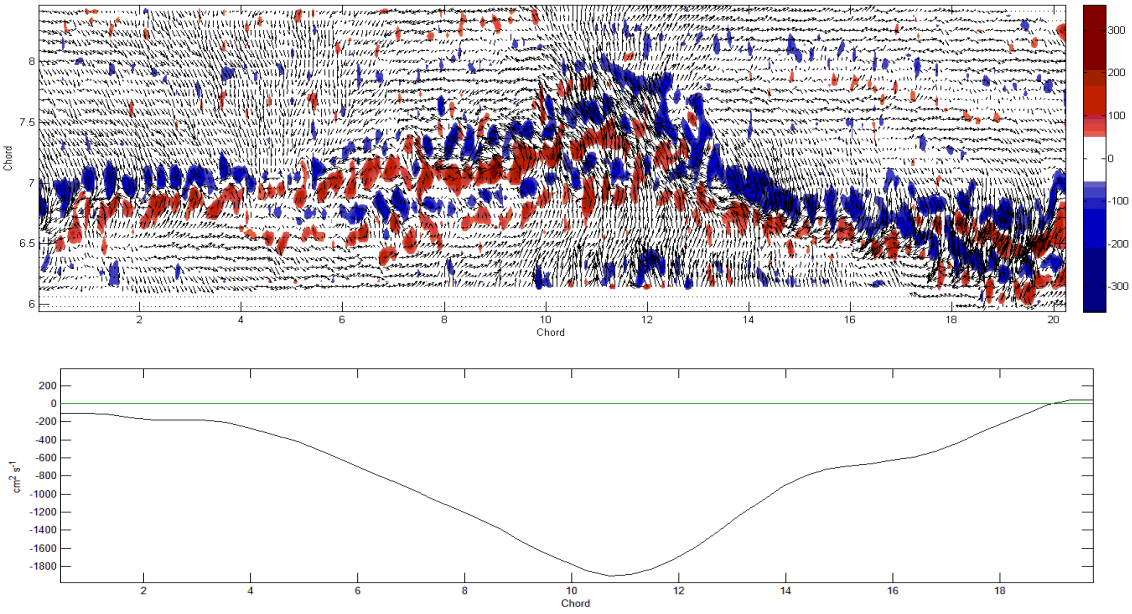

Fig 5b: Sandpiper

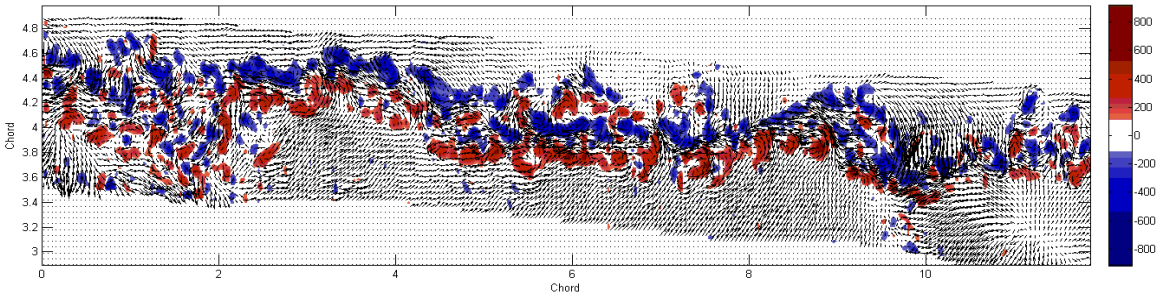

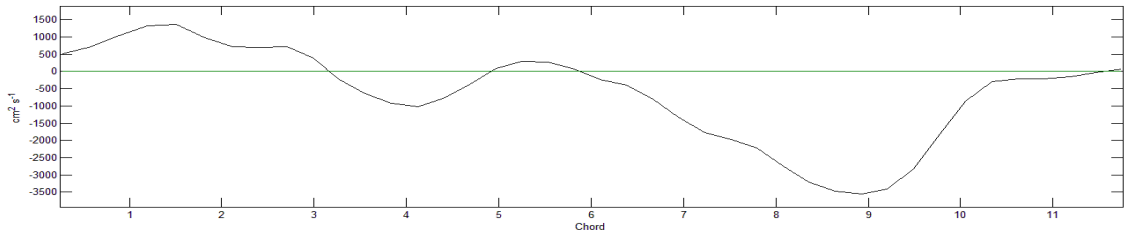

Fig 5c: American robin

Fig 5: Wake reconstruction and cumulative circulation behind freely flying birds during flapping mode, covering a full wingbeat cycle